Title: Reactive oxygen species trigger downward vertical migration in diatom microphytobenthic biofilms as a strategy to cope with oxidative stress

Short title: ROS-Triggered Diatom Biofilm Migration

Authors' information:

1. Alexandre Desparmet[1] (alexandre.desparmet@mnhn.fr ; ORCID 0009-0009-6783-277X)
2. Bruno Jesus[2] (bruno.jesus@univ-nantes.fr ; ORCID 0000-0002-2047-3783)
3. Tony Robinet[1] (tony.robinet@mnhn.fr ; ORCID 0000-0002-3669-2788)
4. Thierry Dufour[3] (thierry.dufour@sorbonne-universite.fr ; ORCID 0000-0002-0397-368X)
5. Cédric Hubas[1] (cedric.hubas@mnhn.fr ; ORCID 0000-0002-9110-9292)

[1]Laboratoire de Biologie des Organismes et Écosystèmes Aquatiques (BOREA), UMR 8067, Muséum National d'Histoire Naturelle, Sorbonne Université, CNRS 7208, IRD 207, UCN, UA, Station Marine de Concarneau, Quai de la Croix, 29900 Concarneau, France.

[2]Institut Des Substances et Organismes de la Mer (ISOMer), UR 2160, Nantes université, Faculté des Sciences et des Techniques, 44000 Nantes, France.

[3]Laboratoire de Physique des plasmas (LPP), UMR 7648, Sorbonne Université, CNRS, École Polytechnique, Univ. Paris-Sud, Observatoire de Paris, Université Paris-Saclay, PSL Research University, 4 Place Jussieu, 75252 Paris, France.

Corresponding author:

Alexandre Desparmet
Laboratoire de Biologie des Organismes et Écosystèmes Aquatiques (BOREA), UMR 8067, Muséum National d'Histoire Naturelle, Sorbonne Université, CNRS 7208, IRD 207, UCN, UA, Station Marine de Concarneau, Quai de la Croix, 29900 Concarneau, France.
alexandre.desparmet@mnhn.fr ; ORCID 0009-0009-6783-277X

ABSTRACT

Diatom-dominated intertidal microphytobenthic biofilms experience daily fluctuations in irradiance, which can lead to oxidative stress within the photosynthetic apparatus through the production and accumulation of reactive oxygen species. To maintain photosynthetic efficiency, benthic diatoms have developed protective strategies, including mobilization of the antioxidant xanthophyll cycle and the ability to migrate vertically through sediments. However, mechanistic understanding of signaling pathways underlying migration remains poorly characterized. This study investigated the triggering effect of reactive oxygen species on behavioral and photophysiological responses through the analysis of lipophilic pigments and fluorescence parameters. To this end, two microphytobenthic communities, one with sediment allowing vertical migration and another without sediment restricting it, were exposed to irradiance, cold atmospheric plasma, and hydrogen peroxide stresses. Results showed a consistent downward migration response under all oxidative stresses, highlighting the key role of reactive oxygen species, especially hydrogen peroxide, in triggering this microphytobenthic behavior. Moreover, a difference was observed between the pathways involved in vertical migration and those underlying photoprotective responses. Hydrogen peroxide and cold atmospheric plasma stresses highlighted the necessity for substantial microphytobenthic migration, whereas irradiance induced a specific and controlled response involving engagement of the xanthophyll cycle, acting in synergy with the migration strategy by showing stronger activation when migration was impaired. By establishing that a rapid and efficient migration could be induced by reactive oxygen species and could act in synergy with the xanthophyll cycle in epipelic cells, this study provides key insights into the molecular basis of microphytobenthic responses to cellular and environmental oxidative stresses.

Key Words: *Diatom microphytobenthic biofilms | Pleurosigma strigosum | Vertical migration | ROS | Light stress | Cold Atmospheric Plasma | Hydrogen peroxide | Xanthophyll cycle | Photophysiology*

Abbreviations: *Diadinoxanthin-Diatoxanthin De-epoxidation state, DES; Minimum dark-adapted fluorescence yield,* F_0*; Maximum quantum yield of photosystem II photochemistry under dark-adapted state, Fv/Fm*; *High light, HL; Hydrogen peroxide, HP; Non-photochemical quenching, NPQ; Cold atmospheric plasma, PL; Relative electrons transport rate, rETR; Reactive oxygen species, ROS; Sediment biofilm, SB; Dark-Adapted control, DA; Without sediment biofilm, WSB; Xanthophyll cycle, XC; Non-regulated non-photochemical quenching energy dissipation, Y(NO); Regulated non-photochemical quenching, Y(NPQ).*

INTRODUCTION

The aquatic microbiome exhibits a remarkable diversity of adaptive strategies to deal with rapid environmental fluctuations. Intertidal sediments, as dynamic interfaces, undergo significant qualitative and quantitative variations in the electromagnetic spectrum throughout the day, impacting the phototrophic communities[1]. Among these, microphytobenthos dominated by epipelic diatoms, forms structured mucilaginous biofilms on muddy substrata, an advantageous lifestyle that plays a key role in their adaptation and associated ecosystem services[2–4].

Light carries essential environmental information that diatoms can perceive either directly through photoreceptors or indirectly via cellular signals, such as levels of reactive oxygen species (ROS) and the redox state of the photosynthetic chain[5–7]. These signals trigger physiological responses involved in light acclimation, photoprotection and photomotile movements, enabling diatoms to acclimate, adapt, and survive[8]. Under high light intensity conditions, photosynthetic capacity can be exceeded, leading to the synthesis and accumulation of ROS, natural by-products of oxygen metabolism, such as singlet oxygen $^1O_2$, superoxide $O_2^{\bullet -}$, hydrogen peroxide H_2O_2 (e.g. via the Mehler reaction), and hydroxyl $HO^{\bullet}$[9]. This deregulation disrupts homeostasis and causes photooxidative damage, such as lipid peroxidation, which compromises cellular integrity[10], and the oxidation of DNA and key proteins such as the photosystem II D1 protein[11, 12], which can ultimately result in cell death[9, 13]. Epipelic diatoms have developed two major adaptive strategies to preempt this ROS formation and accumulation, ensuring optimal photosynthetic processes in a variable light environment: vertical migration behavior and xanthophyll cycle (XC)[14, 15].

First described in 1907 by Fauvel and Bohn, the ability of cells to move vertically through muddy substrata is a behavior regulated both endogenously and plastically by various environmental forcing, such as light information[16–21]. Rapid and temporally adjustable, this actin-myosin-driven gliding system involving the secretion of extracellular mucilage fibrils through the slit raphe, enables diatoms to quickly reposition themselves at low metabolic cost, allowing them to reach sediment layers with optimal irradiance conditions[20–26]. This adaptation, partly responsible for the diversity of Bacillariophyta[27], represents a significant evolutionary advantage and has given rise to distinct migration strategies depending on species, previous light photoacclimation, and the environmental context[15, 17, 19, 20]. In addition, the optimization of diatom light harvesting results from the dynamic regulation of accessory carotenoid pigments, such as xanthophylls linked with the photosystem II Fucoxanthin-Chlorophyll-Protein supercore complex[6, 14, 28, 29]. Overstimulation of the photosynthetic electron transport chain acidifies the thylakoid lumen through proton

translocation associated with the cytochrome b6f complex via the Q-cycle, as well as proton release generated by water photolysis at photosystem II. Under these low-lumen-pH conditions, the enzymatic activity of Diadinoxanthin de-epoxidase is upregulated, leading to the de-epoxidation of Diadinoxanthin embedded in the thylakoid membranes[15, 29–31]. Rapid XC adjustments involved in the energy-dependent component of non-photochemical quenching (qE) are particularly pronounced in diatoms and represent a crucial antioxidant photoprotective response that optimizes thermal dispersion of excess energy in a fluctuating environment, thereby limiting ROS-associated damage in the chloroplast[15, 29–31]. These two major adaptations are complemented by others, such as chloroplast mobility[32, 33], spatial cell orientation[34, 35], frustule nanostructures[36], and cellular ROS management through enzymatic and non-enzymatic antioxidant capacities[31, 37–39]. Together, these adaptations form a sophisticated system that enables diatoms to monitor and respond to environmental fluctuations, contributing to their success in modern marine ecosystems[6].

However, although both diatom vertical migration photoregulation and XC are well characterized individually, the mechanistic understanding of molecular ROS-related cellular signaling pathways that coordinate and integrate real-time protective strategies remain poorly understood in benthic diatoms. The present study, conducted on a natural epipelic microphytobenthic biofilm, addresses this gap by testing the hypothesis that: (1) ROS can act as a trigger signal for downward vertical migration, and (2) ROS-induced migration may be initiated through pathways that operate independently of photoprotection.

MATERIALS AND METHODS

Biofilm sampling and experimental treatments

Microphytobenthos sampling. Microphytobenthos was collected from a disused outdoor breeding pond at the Concarneau Marine Station (France; 47°52’05.85”N; 3°55’00.51”W). The pond retains at least 5 cm of seawater above the sediment at low tide, ensuring that the biofilm developing on fine-grained muddy sediments under a semi-diurnal tidal regime remains permanently immersed (Fig. 1A, B). The upper centimeter of sediment was sampled at low tide on 29 April 2024 (1:00 PM) using a shovel. Muddy samples were placed in plastic boxes with overlying seawater and left to settle under natural ambient laboratory light conditions, without direct illumination, for 24 hours at 20°C.

Community and replicate conditioning. Two communities were compared: one capable of vertical migration through sediment, exhibiting a robust and regular pattern driven by both endogenous circadian and tidal rhythms (Sediment Biofilm, SB), and another in which

vertical movement was impaired due to the absence of sediment (Without Sediment Biofilm, WSB). SB Petri dishes (5.5 cm diameter) were prepared 24 hours before the experiment, whereas WSB Petri dishes were prepared on the day of the experiment from biofilm that had settled in a box for 24 hours. The SB samples consisted of homogeneous sediment discs (5 mm thick) topped with 4 mL of filtered seawater from Concarneau Bay, which were left to settle for 24 hours under ambient laboratory light and temperature. The WSB algal suspension was prepared by gently peeling off the highly cohesive, EPS-rich upper millimeter of the microphytobenthos with tweezers and resuspending it in filtered site seawater (ratio 1 mg : 20 mL). This method minimizes mechanical disturbance and preserves the surface community's cell-size distribution and taxonomic composition. Four milliliters of the WSB suspension were placed in each Petri dish.

Oxidative treatments. Both SB and WSB communities were exposed in the morning (9:00 AM to 1:00 PM), during the biofilm's upward migration phase, to three short oxidative stress treatments. These were compared with dark-adapted controls (DA; <5 µmol photons m^{-2} s^{-1}, which is not complete darkness, but remains below the light compensation point for microphytobenthos[40]). High light (HL) stress was applied to mimic intense irradiance commonly experienced by autotrophic cells in natural environments, with a 30-minute exposure to 1500 µmol photons m^{-2} s^{-1} of full-spectrum warm white LED light panel (supplementary Fig. 1A). A cold atmospheric plasma (PL) was applied for 10 minutes by piezoelectric discharge, using ambient laboratory air as the carrier gas. Exposure was performed indirectly using plasma-activated seawater, with a 3 mm gap maintained between the water surface and the plasma source to prevent mechanical disturbance of diatoms from transient thermal filaments. This treatment generates both reactive oxygen and nitrogen species (*e.g.* H_2O_2, NO_2^-, and NO_3^-), inducing a composite oxidative stress predominantly driven by H_2O_2, which reaches a concentration of 209 µM (additional PL details provided in the supplementary materials and methods). Finally, we applied a targeted hydrogen peroxide stress (HP), consisting of a 10-minute exposure to a 200 µM H_2O_2 seawater solution, allowing the specific effect of this ROS to be isolated. The H_2O_2 concentration was determined based on the amount produced during the 10-minute plasma treatment, ensuring that HP and PL stresses were as comparable as possible. Both HP and PL exposures were conducted in darkness. For sequencing-based community characterization and pigment analyses, five biological replicates ($n = 5$) per community and treatment, all originating from the same initial sampling, were immediately frozen with liquid nitrogen after exposure, lyophilized, and stored at -80°C. Three additional replicates ($n = 3$) were dedicated to photophysiological parameter measurements (Table 1). Additional details on biofilm sampling and experimental treatments are provided in the supplementary materials and methods.

185

186 ***Table 1. Experimental setup***

187 *Summary of the materials and treatments tested in this study.*

Treatments	Dark-Adapted (DA)	High Light (HL)	Cold Atmospheric Plasma (PL)	Hydrogen Peroxide (HP)
Description	Negative control	Natural behavior control	Experimental composite treatment	Positive control
Stress type	-	Warm white UV to near-IR light	Reactive oxygen and nitrogen species stress	Targeted oxidative stress (H_2O_2)
Time exposure	-	30 min	10 min	10 min
ROS origin	-	Endogenous	Exogenous	Exogenous
Experimental materials	Leave in darkness	LED panel Rhino Series (GR-RHINO 260-PRO-DIM)	Plasma activated seawater (PiezoBrush PZ3 with NearField insert from Reylon Plasma GmbH), leave in darkness	Seawater concentrated with H_2O_2 (ref. 216763 from Sigma Aldrich), leave in darkness
Molecular analyses	SB, *n = 5*; WSB, *n = 5*			
Photophysiological measurements	SB, *n = 3*; WSB, *n = 3*			

188

189 ## 18S rRNA gene amplicon sequencing

190 To identify the motile diatoms involved in vertical migration behavior, the eukaryotic
191 microphytobenthic community was characterized through a short-read sequencing on a
192 NovaSeq 6000 System (Illumina). DNA was extracted using the NucleoSpin Soil Mini kit
193 (MACHEREY-NAGEL, ref. 740780.10), and the V4 region of the 18S rRNA gene was
194 amplified using primers TAReuk454FWD1 and TAReukREV3[41]. Library construction and
195 sequencing were performed by the company Biomarker Technologies (BMKGENE) GmbH
196 (Münster, Germany).

197 ## Chlorophyll fluorescence: Pulse Amplitude Modulated fluorometry

198 In order to monitor cellular efficiency under the different treatments and interpret subsequent
199 photoprotective responses, photosynthetic parameters derived from Chlorophyll *a*
200 fluorescence were measured using a MonitoringPen MP 100-E (Photon System
201 Instruments). The light curve program consisted of seven one-minute irradiance steps,
202 increasing from 10 to 1000 µmol photons m^{-2} s^{-1} ($\lambda_{LED\ excitation}$ = 470 nm), with consistent gain,
203 superpulse, and flashpulse intensity settings maintained across all measurements. The initial
204 linear α-slope, representing the maximum light use efficiency of photosystem II, was derived
205 from the light-use-efficiency photosynthesis-irradiance (P-E) curves using a previously

206 described and modified model[42, 43]. The relative electron transport rate (rETR) of
207 photosystem II, an indicator of productivity[23] and in some cases a proxy for carbon
208 fixation[44], corresponds to the values extracted directly from light curve points. The
209 maximum quantum yield of photosystem II photochemistry under dark-adapted state
210 (Fv/Fm), as well as non-photochemical quenching (NPQ) and its regulated Y(NPQ) and non-
211 regulated Y(NO) components, were calculated using established equations[45, 46]
212 (supplementary Table 1). All fluorescence measurements of photosynthetic parameters for
213 each sample and treatment were performed twice: once before and once after stress
214 exposure, each time following a minimum dark adaptation period of 10 minutes. For HL,
215 post-stress measurements were taken after this dark adaptation period once the exposure
216 had ended, whereas for HP and PL, measurements were performed immediately after the
217 10-minute stress period, as the samples were already dark-adapted under these treatments.
218 For the DA controls, which do not receive any stress treatment, measurements were
219 performed in parallel with the experimental samples, ensuring that they were in the same
220 temporal framework.

221 **Monitoring of vertical migration**

222 In addition, to assess the vertical migratory response over time, the minimum fluorescence of
223 dark-adapted samples (F_0), used as a proxy of surface algal biomass[14, 17], was monitored
224 in the SB community after a 24-hour settling period under ambient laboratory light and
225 temperature. F_0 measurements were conducted independently and randomly on dense
226 biofilms (182 cm²) contained in 14 × 13 cm boxes (one box per stress), then compared with
227 their respective DA biofilms (HL and PL: $n = 8$; HP: $n = 5$). Due to the rapid induction of the
228 migratory response in microphytobenthos, F_0 biomass monitoring was resumed after 5
229 minutes of dark adaptation following the end of HL stress, and immediately after HP and PL
230 stresses.

231 **Lipophilic pigments analysis**

232 To characterize the metabolic impact of the treatments and complement the photosynthetic
233 efficiency data, the lipophilic pigments were extracted according to a previously published
234 method[47]. Freeze-dried samples (10 mg WSB, 40 mg SB) were incubated for 15 minutes
235 at -21°C in 2 mL of 95% methanol buffered with 2% ammonium acetate, then filtered through
236 a 0.2µm PTFE filter. Aliquots of 100 µL were injected into an Agilent 1260 Infinity HPLC
237 system equipped with a C18 Supelcosil column and a UV-VIS photodiode array detector
238 (DAD 1260 VL, 250-900 nm). The method employed a flow rate of 0.6 mL min^{-1} using solvent
239 mixture A (0.5M ammonium acetate in 85:15 methanol:water), B (90:10 acetonitrile:water),

240 and C (100% ethyl acetate). A total of 44 microphytobenthic pigments were detected (list and
241 abbreviations are provided supplementary Table 2), and their concentrations (µg pigment g^{-1}
242 dry weight) were quantified using calibration curves based on phytoplankton pigment
243 standards from DHI. Two groups of derived Chlorophyll *a* were identified: the "Chlorophyll *a*-
244 derivatives" group includes unidentified Chlorophyll *a*-like pigments, as well as the allomer,
245 and epimer forms; the "Pheopigments" group includes Pheophytins *a*, Pheophorbides *a*, and
246 Pyropheophytin *a*. The contribution (%) of each Chlorophyll *a*-derivatives and Pheopigments
247 group to the total Chlorophyll *a* pool was calculated by dividing their concentrations by the Σ
248 $_{[\text{Chlorophyll } a]}$ concentration, used as a proxy of biomass ($\Sigma_{[\text{Chlorophyll } a]}$ = [Chlorophyll *a*] +
249 [Chlorophyll *a*-derivatives] + [Pheopigments]). The de-epoxidation state (DES %), defined as
250 the ratio of Diatoxanthin to the Diadinoxanthin + Diatoxanthin pool, was calculated as
251 [Diatoxanthin]/([Diadinoxanthin] + [Diatoxanthin]) x100.
252 Additionally, pigment concentrations were used to reconstruct the microphytobenthic
253 community absorption spectrum for Qphar estimation, thus providing a more accurate
254 assessment of light actually absorbed by diatoms at the substrata surface during HL
255 treatment (supplementary Fig. 1B-E; see supplementary materials and methods).

256 Data treatment

257 Raw 18S rRNA gene amplicon sequencing data were processed via the SAMBA workflow to
258 generate amplicon sequence variants, which were assigned taxonomically with the PR2
259 (v5.0.0) database. Reads were normalized by coverage-based rarefaction and transformed
260 to relative abundances. Diversity between communities was tested using the Wilcoxon rank-
261 sum test.
262 For both communities, the net impact values of stress ($\Delta_{\text{After-Before}}$) on photophysiological
263 parameters were calculated and compared to those of the DA, which accounts for metabolic
264 drift over time, using Welch's two-sample t-test.
265 Pigment composition was analyzed using ANOSIM tests based on Euclidean distances
266 between individual coordinates. These were extracted from the first two axes of each PCA
267 performed on Hellinger-transformed pigment concentrations to assess the significant effects
268 of treatments and communities. A Between-Class Analysis was performed to characterize
269 the effects of the stress factor on the total inertia of pigment profiles for both communities. A
270 SIMPER analysis on relative proportions, performed independently for each SB and WSB
271 community, was used to identify pigments that varied significantly under each stress
272 compared to DA. Changes in pigment ratios were tested using the Mann-Whitney U test.

273 # RESULTS

274 ## Motile diatom *P. strigosum* dominates the eukaryotic microphytobenthic
275 community

276 Despite inherent biases, such as the amplification of free eDNA or the underrepresentation of
277 rare species in communities[48], the sequencing approach provided a relevant semi-
278 quantitative overview of the biovolume-dominant eukaryotic microphytobenthic taxa. The two
279 communities displayed distinct assemblages, with significantly lower diversity indices and
280 reduced variability among WSB replicates compared with SB (Wilcoxon-Mann-Whitney, $P <$
281 0.05) (supplementary Fig. 2). The eukaryotic community was dominated by
282 *Bacillariophyceae*, *Nematoda*, and *Arthropoda*, with an expected increase in the relative
283 proportion of *Bacillariophyceae* in WSB, due to the substrata surface layer subsampling
284 protocol which excluded much of the sediment-associated diversity (Fig. 1D). Autotrophic
285 biovolume was largely dominated by the raphid species *Pleurosigma strigosum*, which
286 accounted for 88.7% of WSB relative abundances, together with other benthic diatoms, such
287 as the genera *Navicula* and *Gyrosigma* (possibly *G. balticum*[49]) (Fig. 1C, E).
288

289 ## Downward vertical migration triggered under the three stresses

290 Vertical migration was assessed by tracking F_0 measurements under HP-, PL-, and HL-
291 induced ROS stresses. F_0 serves as a proxy for biomass, effectively reflecting the motile
292 behavior of benthic diatoms[17]. Indeed, in WSB treatments, F_0 levels did not decrease
293 compared to DA following exposure to HP, PL, and HL stresses (supplementary Tables 3
294 and 4). In addition, Fv/Fm values remained stable for HP and PL treatments. Altogether,
295 these results rule out potential Chlorophyll *a* bleaching and the induction of karyostrophy
296 under any of the three stresses[32, 33].
297 Regardless of how ROS were produced or applied, the *P. strigosum* dominated biofilms
298 sensed both metabolic and environmental oxidative stresses, responding with a marked
299 downward migration (Fig. 2). This was quickly followed by a gradual recovery of surface
300 biomass under all stresses as soon as the stress ended. The intensity of the behavioral
301 response varied according to the type of stress, with exogenous ROS triggering the strongest
302 effect. In particular, HP induced a clear and rapid on/off switch-migration within
303 approximately one minute (experimental observation), with a 75.5% decrease in F_0, followed
304 by PL causing a 35.6% decrease and HL an 8.9% reduction (Table 2). Within this framework,
305 the fastest return of biomass at the sediment surface occurred under HP, with a +116% F_0
306 min^{-1} recovery slope, compared with +67% for HL and +47% under PL, respectively.
307

308 ***Table 2. Extent of the behavioral response of the microphytobenthic surface biomass***
309 *Table reporting changes in F_0 (data from Fig. 2), at the sediment surface (average ± SD, arbitrary*
310 *unit), before and after treatments, for the Sediment Biofilm (SB) samples (n = 8 for HL and PL; n = 5*
311 *for HP). DA [(1)], DA [(2)], and DA [(3)] correspond to Dark-Adapted control samples measured in parallel to*
312 *the HL, HP, and PL experimental treatments, respectively. The Δ After-Before (a.u.) and Changes (%)*
313 *columns summarize the temporal evolution of surface F_0. The post-stress recovery slope is calculated*
314 *using a linear regression model applied to F_0 fluorescence kinetics over 60 minutes after stress*
315 *cessation, as an indicator of microphytobenthos resilience. The slope reflects the rate of F_0 variation*
316 *per minute during recovery (F_0 min^{-1}).*

Treatments	F_0 Before (a.u.)	F_0 After (a.u.)	Δ After-Before (a.u.)	Changes (%)	Recovery slope (F_0 min^{-1})
DA [(1)]	12752 (1606)	14540 (787)	+1788	**+14%**	**+11**
HL	13080 (807)	11916 (993)	-1164	**-9%**	**+67**
DA [(2)]	11393 (1457)	12232 (703)	+839	**+7%**	**-2**
HP	11546 (1100)	2824 (433)	-8722	**-76%**	**+116**
DA [(3)]	15263 (726)	14906 (945)	-356	**-2%**	**+17**
PL	15496 (843)	9979 (1801)	-5517	**-36%**	**+47**

317

318 Divergent photophysiology: Exogenous ROS oxidize pigments with limited 319 photosynthetic impairment vs. HL-driven photoinhibition

320 To complement the finding that microphytobenthic vertical migration behavior may be
321 triggered by ROS, we assessed the metabolic cost associated with these stresses by
322 examining the functional response of the photosynthetic apparatus. To this end, key
323 photosynthetic parameters and lipophilic pigment data were monitored in both communities.
324 Unlike SB, the WSB samples capture the impact on the most complete and intact community
325 possible, as supported by the sequencing results, without the possibility of mitigation through
326 migratory responses.
327 Before stress exposure, all replicates across all treatments showed high initial Fv/Fm values
328 (> 0.67) and high initial α-slope values (> 0.32), indicating that the cells were in an optimal
329 physiological state. In both communities, post-exposure photosynthetic efficiency values
330 remained high under all three stresses. This was particularly true for exogenous stresses in
331 WSB, where despite the inability to mitigate stress through migration, the cells maintained
332 high Fv/Fm and α-slope values (> 0.66 and > 0.33, respectively). Taken together, these
333 results support that, as for HL, the intensities of HP and PL stresses remained within the
334 photophysiological tolerance range of the cells despite their inability to migrate, thereby
335 enabling reliable interpretation of the data.
336 The SB community showed a general decrease in photosynthetic efficiency under all three

stresses, characterized by a significant drop in the α-slope and Fv/Fm values (Welch's two-sample t-test, $P < 0.05$). An effective photoprotective response was observed exclusively under HL, with increases in NPQ^{1000} and $Y(NPQ)^{1000}$ values, indicating controlled dissipation of excess energy (Fig. 3; supplementary Fig. 3). Conversely, stress exposure in WSB revealed a marked photophysiological impact only under HL, with a drop in Fv/Fm values, along with a strong activation of the effective photoprotection Y(NPQ) and an increase in unregulated photoinhibition $Y(NO)_{m\ obs}$. The increase in this uncontrolled dissipation component reflects an excess of irradiance delivered by HL, and absorbed by the cells, estimated at ~519 µmol photons m^{-2} s^{-1} by Qphar and recalculated at ~448 µmol photons m^{-2} s^{-1} when accounting for the cell pigment packaging effect. HP and PL did not significantly alter the state of the photosynthetic electron transport chain, as particularly evident when comparing the photosystem II quantum yield response curves (Fig. 4). Nevertheless, the exogenous PL stress appeared more impactful than HP, highlighted by a decrease in $rETR_{m\ obs}$ in both SB and WSB communities.

Microphytobenthic lipophilic pigment analyses revealed diatom-typical profiles in all samples, with the DA WSB treatment providing the most representative unstressed baseline composition: Chlorophyll *a* and its derivatives (58.3%), Fucoxanthin and its derivatives (28%), Chlorophyll *c2* (6.7%), Diadinoxanthin + Diatoxanthin (2.4%), ββ + βε-carotene (1.3%) (supplementary Fig. 4). Both communities were characterized by a clear difference in their pigment compositions (ANOSIM, R = 1; P = 1e-04, supplementary Fig. 5A). This was due to higher relative proportions of Chlorophyll *a*, Fucoxanthin, and Chlorophyll *c2* in WSB samples, whereas SB samples exhibited an increase in degraded forms such as Pheopigments, Unknown-carotenoids, or Fucoxanthin-like. Within both communities, stresses significantly affected pigment profiles (SB ANOSIM R = 0.82, P = 1e-04, supplementary Fig. 5B and WSB ANOSIM R = 0.73, P = 1e-04, supplementary Fig. 5C), which explain 84% and 67% of the total inertia observed in the SB and WSB samples, respectively (supplementary Fig. 6). SIMPER analyses revealed a stronger impact of exogenous stresses on pigment composition compared to HL in both communities, with a greater number of significantly affected pigments relative to DA (SIMPER, $P < 0.05$). This was particularly evident in SB samples, where 3, 17, and 39 pigments were significantly affected under HL, HP, and PL, respectively, compared to 10, 15, and 16 pigments in WSB samples. This differential impact of the stressors was mainly driven by Chlorophyll *a*-derivatives rather than Pheopigments (Fig. 5B, C), suggesting that HP and PL caused a broader and untargeted effect, with direct oxidation of numerous pigments despite short exposure times, whereas HL represented a more targeted stress. The latter was particularly characterized by the activation of XC, with significant increases in the DES, especially in

374 WSB, where average de-epoxidation rates exceeded 46% (Fig. 5A, concentrations detailed
375 in supplementary Table 5). Finally, WSB samples showed the same impact dynamics on
376 Chlorophyll *a*-derivatives as SB, confirming that the stresses differentially affected the
377 surface motile diatoms themselves.

378 DISCUSSION

379 HL-induced vertical migration in microphytobenthos

380 Pigment profiles provided a chemotaxonomic signal typical of diatoms, characterized by high
381 fucoxanthin content together with Chlorophyll *c2* and Chlorophyll *a*[28], which corroborated
382 the sequencing results (Fig. 1E). Both communities were characterized by a biovolume
383 dominated by benthic diatoms, especially *Pleurosigma strigosum*, along with other
384 autotrophs and meiofauna (*e.g.* nematodes, copepods, and ostracods), corroborating
385 previous microscopic observations[49] and literature on microphytobenthos in similar
386 environments[50, 51]. In line with these observations, the motile behavioral response,
387 pigmentary mobilization, and photophysiological signals can be largely attributed to the
388 benthic diatoms dominating the surface biovolume, with *P. strigosum* playing a predominant
389 role.
390 In SB experiments, exposure of the microphytobenthos to 1500 µmol photons m^{-2} s^{-1} for 30
391 minutes induced a moderate decrease in F_0, indicating a shift in biofilm dynamics from
392 upward to downward migration (Fig. 2). This response was reversible, with biomass returning
393 to the surface after the treatment ended. Vertical migration in benthic diatoms is governed by
394 self-sustained circadian and tidal rhythms that require regular resetting to remain
395 synchronized[20, 52]. These rhythms are further modulated by environmental cues, allowing
396 rapid and temporally adjustable responses[18, 21, 23]. The induction of a HL-driven vertical
397 migration strategy through muddy substrata was expected and is well documented in many
398 autotrophic microorganisms, including *P. strigosum*, highlighting a relatively common
399 evolutionary advantage[17, 20, 26]. To maintain optimal cellular performance and cope with
400 ROS, this migratory response operates in synergy with other photoprotective mechanisms
401 that collectively sustain cellular fitness[6].

402 Migration and photoprotection act synergistically under HL-induced ROS

403 In parallel to the downward migration, a decline in photosynthetic efficiency was observed in
404 HL-treated SB samples, suggesting that vertical migration did not maintain short-term
405 photosynthetic performance. This decline was likely caused by an increase in Y(NPQ) due to
406 targeted DES-XC mobilization (Fig. 3 and 5A), combined with slight photoinhibition,
407 consistent with previous reports[26, 53]. Irradiance is known to generate both endogenous

408 and exogenous ROS-high-oxidative-potential molecules that can cross membranes and act
409 as signaling agents across multiple subcellular compartments[6, 9, 54–59]. Diatoms must
410 cope with them, as excessive accumulation poses deleterious risks, including the oxidation of
411 essential photosynthetic components[10, 11]. To prevent ROS formation, HL can rapidly
412 trigger effective Y(NPQ) supported by the Diadinoxanthin + Diatoxanthin xanthophyll pool,
413 where overstimulation of the photosynthetic electron transport chain induces lumen
414 acidification, upregulating the pH-sensitive diadinoxanthin de-epoxidase enzyme[15, 30, 60].
415 Here, both vertical migration and XC activation likely limit ROS production and accumulation,
416 indicating that all components of a typical and effective photoprotection strategy are
417 engaged, as expected for benthic intertidal diatoms under photooxidative stress. In addition,
418 diatoms actively regulate cellular redox balance under light-induced ROS via both enzymatic
419 and non-enzymatic antioxidant capacities, including upregulation of superoxide dismutase
420 and ascorbate peroxidase[37, 39, 61], mobilization of antioxidant non-protein thiols and
421 glutathione pools[62], or by direct ROS scavenging by carotenoids[29, 31, 38].
422 Although Chlorophyll *a* fluorescence is generally a reliable indicator of cellular physiological
423 state under various abiotic stresses[63], the presence of a sedimentary environment in SB
424 can alter the signal (*e.g.* cell reorientation, effective light exposure, or downward migration,
425 potentially leaving fewer viable cells at the surface). Consequently, SB photosynthetic
426 parameters must be interpreted with caution[45, 64]. WSB results help to overcome this
427 potential bias, thereby clarifying the synergy between the need for migration, the XC
428 activation, and the photosynthetic efficiency. WSB cells, unable to adjust their vertical
429 position, displayed a stronger increase in DES, as an HL-compensatory response (Fig. 5A).
430 Enhanced XC mobilization is a well-described compensatory response in diatoms with
431 impaired motility, as shown under light exposure combined with latrunculin motility
432 inhibitors[14, 26, 65]. In natural environments, this trade-off becomes evident when
433 comparing DES activation in epipsammic diatoms, which inhabit brighter environments
434 where vertical migration is limited, resulting in a stronger response than in epipelic
435 diatoms[65–67]. Despite the XC response in WSB, an increase in Y(NO) indicates that the
436 stress still induced a slight unregulated photoinhibition from the lowest irradiances of the light
437 curves (Fig. 4).
438 In fact, HL induced finely tuned and metabolically controlled cellular adjustments, involving
439 subtle pigment remodeling as part of a photoprotective strategy, which works in synergy with
440 vertical migration behavior. However, although this targeted response is likely driven by
441 intracellular variations (e.g. metabolic imbalances resulting from ROS accumulation primarily
442 due to light, and potentially in combination with other stresses, such as temperature, pH,
443 exposure to toxic substances, or nutrient availability), migration may also result from
444 environmental oxidative signals[58]. These include exogenous HL-ROS generated by

445 photooxidation of dissolved organic matter in muddy substrata[56, 58, 68], and ROS actively
446 or passively released by neighboring cells in the biofilm, leading to their local
447 accumulation[13, 54, 69]. Moreover, precipitation can deliver water containing up to 85 µM
448 H_2O_2[58]. All these conditions in intertidal environments can rapidly and transiently increase
449 exogenous oxidative stress for microphytobenthos, an environmental scenario not far from
450 the HP and PL treatments, although these stresses involve higher concentrations than those
451 typically measured in tidal zones[56].

452 Exogenous ROS induce untargeted oxidative stress on diatoms

453 As for HL-induced photooxidation, exogenous ROS generated by HP and PL, including H_2O_2,
454 likely interacted with sedimentary dissolved organic matter, triggering chemical reactions.
455 These reactions could alter oxidative conditions in SB, including potential acidification that
456 may explain the DES increase. This XC activation in SB appeared to occur without
457 development of regulated Y(NPQ) (supplementary Fig. 3). As previously discussed,
458 downward vertical migration into the sediment can strongly interfere with fluorescence
459 measurements, including underestimation of NPQ[45, 64]. In addition, migration of viable
460 cells into deeper sediment layers may leave senescent or physiologically impaired cells at
461 the surface, further altering the residual fluorescence signal. This interpretation is supported
462 by the higher relative abundance of Pheopigments observed in SB compared to WSB
463 samples (Fig. 5C), along with the increase in Y(NO), concomitant with the apparent loss of
464 Y(NPQ) development capacity. Due to the substantial downward migration of biomass, the
465 reliability of surface fluorescence measurements in SB is intrinsically compromised, and it is
466 therefore not possible to definitively conclude whether the observed signal reflects a reduced
467 and physiologically altered surface population or whether the induced diatoxanthin is
468 preferentially used in antioxidant functions rather than photoprotective NPQ[38].
469 In fact, exogenous stresses in both communities exhibited a stronger untargeted oxidizing
470 capacity, leading to extensive and differential oxidation of the pigment system. The presence
471 of sediment, potentially creating altered oxidative conditions in SB, combined with an
472 associated pool of degraded Pheopigments, could explain the higher Between-Class
473 Analysis explained inertia values observed for SB (Supplementary Fig. 6). The global impact
474 of HP and PL is particularly reflected in the oxidation of Chlorophyll *a* into Chlorophyll *a*-
475 derivatives (Fig. 5B), suggesting a random and direct oxidation of lateral chains of
476 Chlorophyll *a* molecules[70]. Some of these alternative forms of Chlorophyll *a* may have
477 cellular functions[9, 29, 71], and their accumulation may serve as an indicator of
478 environmental conditions[5]. Despite PL stress inducing a higher accumulation of Chlorophyll
479 *a*-derivatives, indicating more detrimental conditions than HP, both exogenous stresses
480 resulted in high post-stress photosynthetic performance. This supports the relevance of the

481 applied stress intensities, as structural modifications in part of the Chlorophyll *a* pool did not
482 prevent the maintenance of light-harvesting functions, even when migration was impaired.

483 Vertical migratory behavior triggered by exogenous ROS

484 Our results showed that brief exposure to HP- and PL-ROS had a moderate impact on
485 photophysiology (Fig. 4), while simultaneously triggering a rapid downward vertical migration
486 (Fig. 2). Reported migration velocities are highly variable, typically ranging from 1 to 30 µm s^{-}
487 ^{1} for horizontal movements, and generally lower for vertical displacements, generally
488 between 0.17 and 0.28 µm s^{-1} [17, 20, 21, 24]. Based on these values, diatoms could
489 theoretically migrate vertically by approximately 102 µm and 168 µm under our 10-minute
490 stresses, reaching muddy layers where light availability is reduced by ~66%[65], which is
491 consistent with the strong decrease observed in F_0. In both cases, stresses did not
492 compromise the motility of diatoms, which rapidly initiated an upward migration once the
493 stresses ended, as shown by post-stress recovery slope (Table 2). This plasticity in
494 behavioral response, which adjusts in real time to changing surface conditions, was
495 nevertheless more affected under PL, with a slower return of biomass, indicating that PL
496 represented a harsher stress. ROS, such as H_2O_2, are described in literature as secondary
497 messengers that mediate signal transduction and activate defense mechanisms during
498 adaptation to both biotic and abiotic stress[5, 6, 8, 59], including motile capacities in
499 microalgae[25, 55, 57, 72, 73]. The hypothesis that ROS are one of the components inducing
500 migration under a composite stress such as PL is corroborated by the strong migration
501 observed under the positive control HP, which specifically isolates the effect of H_2O_2. This
502 molecule has been widely used in previous studies to investigate its role as a driver in
503 various cellular pathways in microalgae[59, 72, 74–77], as exogenously applied H_2O_2 can
504 accumulate intracellularly via transmembrane diffusion through aquaporins[78]. The results
505 presented here demonstrate its key role as a strong on/off trigger of the transient motile
506 response. Moreover, the behavioral response did not reflect the impact of exogenous
507 stresses on the pigment system, as the strongest mobilization occurred under HP rather than
508 under PL.
509 Together, these results suggest that vertical migration could be triggered by ROS, especially
510 H_2O_2, without necessarily being associated with a decline in photosynthetic performance. In
511 other words, the presence of ROS, even in darkness and without impaired photosynthetic
512 capacity, is sufficient to trigger downward motility. This triggering of migration occurs without
513 inducing an effective controlled photoacclimatory Y(NPQ) response involving XC. Exogenous
514 ROS likely acted through a sophisticated signal transduction network to trigger this rapid and
515 essential motility response of the microphytobenthos under harmful oxidative environmental
516 conditions[6, 8]. The precise cellular pathways by which H_2O_2 act, either directly or indirectly,

517 to trigger this behavior remain uncertain in benthic diatoms and require further investigation.
518 Nevertheless, certain studies in the literature provide a solid foundation for preliminary
519 research.

520 Do ROS induce calcium signaling underlying motility?

521 In benthic pennate diatoms, gliding motility is driven by an actin-based cytoskeletal system
522 organized along the apical axis. This system transmits force through transmembrane
523 complexes to mucopolysaccharide microfibrils secreted via the raphe slit, thereby enabling
524 adhesion and traction on substrata[20, 22]. ROS can plausibly act on several components of
525 the gliding system, including cytoskeletal reorganization, adhesive mucilaginous compounds,
526 ATP availability, gene expression, or by generating oxidized metabolites that function as
527 infochemicals and secondary messengers in specific signaling pathways (*e.g.* oxylipins, thiol
528 compounds)[12, 22, 79–83]. Nevertheless, a migration behavior primarily controlled by ROS-
529 calcium signaling remains one of the most prominent hypotheses, both of them being central
530 components of microalgal adaptation to environmental stressors[84].
531 Recent studies have shown that disruption of the transthylakoid proton gradient inhibits
532 motility in benthic diatoms, potentially through effects on calcium homeostasis, thereby
533 suggesting a broader link between behavior and high light-driven photoprotection[77, 85].
534 Our results provide experimental evidence that diatom migration can be triggered in
535 darkness and independently of an effective Y(NPQ) response, further refining the regulatory
536 cascade underlying this behavior by linking ROS to an “oxidotactic” motility that may involve
537 calcium signaling. Elevations of stromal Ca^{2+} have been reported in response to intracellular
538 ROS accumulation under high light and after exogenous H_2O_2 exposure[76, 77]. In plants,
539 both endogenous H_2O_2 accumulation and exogenous H_2O_2 exposure induce Ca^{2+} influx via
540 calcium channel activation[86], an influx implicated in controlling diatom migration[87, 88]
541 and, more recently, contributing to gliding motility through EukCatAs ion channels that
542 regulate cytosolic Ca^{2+} levels[89]. In addition, it has been shown that certain membrane
543 receptor kinases can directly sense extracellular H_2O_2 and initiate Ca^{2+} channel opening
544 without a prior intracellular H_2O_2 accumulation[90]. In the environment, exposure to copper
545 promotes oxidative stress and intracellular Ca^{2+} perturbations alongside active gliding
546 motility[25], and new evidence has identified a bistability in phytoplanktonic microalgae, in
547 which vertical migration switches are driven by a ROS-induced oxidative stress threshold[72].
548
549 Our study does not provide a definitive conclusion on the full role of ROS, such as H_2O_2.
550 Nevertheless, these results, supported by recent literature, help to identify the major putative
551 components underlying the cellular signaling of this behavior (Fig. 6). Although detailed
552 information on the ROS-Calcium-Motility interplays is still lacking, particularly regarding how

553 the calcium acts on the locomotion machinery pathways, we propose that certain rapid
554 responses to environmental cues, such as a vertical migratory behavior switch observed in
555 this experiment, are mediated, at least in part, by a ROS-sensing system.

556 CONCLUSION

557 All results provide strong evidence for the key role of ROS, particularly H_2O_2, as a critical
558 signaling molecule triggering the rapid motile behavior in diatom-dominated
559 microphytobenthic biofilms. The strongest downward migration occurred under exogenous
560 stresses that minimally impacted photosynthetic efficiency, despite a broad and untargeted
561 oxidative stress on pigments. Moreover, these exogenous stresses were unable to induce an
562 effective, controlled photoprotective response, as reflected by Y(NPQ). This demonstrates
563 that exposure to H_2O_2 alone, in the absence of any light cue, is sufficient to trigger a plastic
564 motility. Such a response suggests a signaling pathway that may operate independently from
565 those governing photophysiology, thereby broadening the ecological relevance of vertical
566 migration in a multi-stress environmental context. This stress-mitigation strategy can act
567 synergistically with pigments under high irradiance in natural environments, as supported by
568 the enhanced activation of the XC when migration was restricted. Together, the findings
569 corroborate previous studies showing that vertical migration is an important adaptive trait
570 allowing diatoms to regulate homeostasis and support long-term physiological performance.

571 Overall, these findings provide evidence of the importance of ROS signaling in shaping
572 microphytobenthic motility, demonstrating that benthic diatoms can monitor both metabolic
573 and environmental ROS. This ROS-mediated early warning sensing system likely represents
574 an adaptive strategy that enables efficient surveillance of environmental conditions, allowing
575 cells to rapidly prevent deleterious conditions, maintain cellular fitness, and ultimately support
576 the ecological success of diatoms in highly variable environments. This offers new insights
577 into how oxidative stress regulates autotrophic life and more broadly highlights its key role
578 within the aquatic microbiome. The response to oxidative challenges likely relies on a
579 complex signaling cascade that requires further in-depth investigation to identify potential
580 effectors in ROS-motility signaling and clarify how triggering this behavior allows cells to
581 cope with oxidative stress in natural environments.

582

583

584

ACKNOWLEDGMENTS

Our thanks go to Johann Lavaud for his valuable discussions on photophysiology. We are also thankful to Manon Leroux for her essential assistance in the laboratory during the experiment. We acknowledge the chromatography and mass spectrometry facility at the Concarneau Marine Station (PtSMB-MNHN) for providing access to the HPLC.

CONFLICTS OF INTEREST

The authors declare no conflict of interest.

FUNDING

This work was funded by the Institut de l'Océan from the Sorbonne University alliance and the Muséum national d'Histoire naturelle.

DATA AVAILABILITY

All scripts used to generate the figures and perform the analyses are available on GitHub, and are also archived on Zenodo. The datasets generated and analyzed during the current study are available in the Zenodo repository. The raw sequencing data have been deposited in the European Nucleotide Archive (ENA) under project accession number **ERA33152396** (Experiments **ERX14500286 – ERX14500369**; Runs **ERR15095684 – ERR15095767**) and can be accessed via the ENA portal. The raw chromatogram files used for pigment analyses are available in the Zenodo repository.

AUTHOR CONTRIBUTIONS

AD: Conceptualization, Methodology, Investigation, Data curation, Formal analysis, Visualization, Writing - original draft. BJ: Data curation, Formal analysis, Validation, Writing - review & editing. TR: Data curation, Methodology, Formal analysis. TD: Resources, Methodology, Writing - review & editing. CH: Supervision, Methodology, Data curation, Formal analysis, Validation, Writing - review & editing.

REFERENCES

1. Kühl M, Jorgensen BB. The light field of microbenthic communities: radiance distribution and microscale optics of sandy coastal sediments. *Limnol Oceanogr* 1994;39:1368–1398. 10.4319/lo.1994.39.6.1368

614 2. Underwood GJC. Microphytobenthos. Encyclopedia of Ocean Sciences. Academic
615 Press, 2001, 1770–1777. 10.1006/rwos.2001.0213
616 3. Pinckney JL. A mini-review of the contribution of benthic microalgae to the ecology of the
617 continental shelf in the South Atlantic Bight. *Estuaries coast* 2018;41:2070–2078.
618 10.1007/s12237-018-0401-z
619 4. Hubas C, Passarelli C, Paterson DM. Microphytobenthic biofilms: composition and
620 interactions. In: Beninger PG (ed.), Mudflat Ecology. Cham: Springer International
621 Publishing, 2018, 63–90. 10.1007/978-3-319-99194-8_4
622 5. Waszczak C, Carmody M, Kangasjarvi J. Reactive oxygen species in plant signaling.
623 *Annu Rev Plant Biol* 2018;69:209–236. 10.1146/annurev-arplant-042817-040322
624 6. Falciatore A, Mock T (eds). The molecular life of diatoms. Cham: Springer International
625 Publishing, 2022. 10.1007/978-3-030-92499-7
626 7. Duchêne C et al. Diatom phytochromes integrate the underwater light spectrum to sense
627 depth. *Nature* 2025;637:691–697. 10.1038/s41586-024-08301-3
628 8. Lepetit B, Dietzel L. Light signaling in photosynthetic eukaryotes with ‘green’ and ‘red’
629 chloroplasts. *Environ Exp Bot* 2015;114:30–47. 10.1016/j.envexpbot.2014.07.007
630 9. Foyer CH, Hanke G. ROS production and signalling in chloroplasts: cornerstones and
631 evolving concepts. *Plant J* 2022;111:642–661. 10.1111/tpj.15856
632 10. Doose C et al. Non-enzymatic oxylipin production in a mudflat microphytobenthic biofilm:
633 evidence of a diatom response to light. *Front Photobiol* 2024;2:1441713.
634 10.3389/fphbi.2024.1441713
635 11. Nishiyama Y, Allakhverdiev SI, Murata N. A new paradigm for the action of reactive
636 oxygen species in the photoinhibition of photosystem II. *Biochim Biophys Acta Bioenerg*
637 2006;1757:742–749. 10.1016/j.bbabio.2006.05.013
638 12. Knieper M, Viehhauser A, Dietz K-J. Oxylipins and reactive carbonyls as regulators of the
639 plant redox and reactive oxygen species network under stress. *Antioxidants*
640 2023;12:814. 10.3390/antiox12040814

641 13. Mittler R et al. ROS signaling: the new wave? *Trends Plant Sci* 2011;16:300–309.
642 10.1016/j.tplants.2011.03.007
643 14. Serôdio J et al. Efficiency of photoprotection in microphytobenthos: role of vertical
644 migration and the xanthophyll cycle against photoinhibition. *Aquat Microb Ecol*
645 2012;16:161–175. 10.3354/ame01591
646 15. Blommaert L. Photoprotection in intertidal benthic diatoms. 2017;Ph.D. dissertation.
647 Ghent University. Faculty of Sciences, Ghent, Belgium.
648 16. Fauvel P, Bohn G. Le rythme des marées chez les diatomées littorales. *CR Soc Biol*
649 1907;62:121–123.
650 17. Consalvey M, Paterson DM, Underwood GJC. The ups and downs of life in a benthic
651 biofilm: migration of benthic diatoms. *Diatom Res* 2004;19:181–202.
652 10.1080/0269249X.2004.9705870
653 18. Coelho H, Vieira S, Serôdio J. Endogenous versus environmental control of vertical
654 migration by intertidal benthic microalgae. *Eur J Phycol* 2011;46:271–281.
655 10.1080/09670262.2011.598242
656 19. Barnett A et al. The vertical migratory rhythm of intertidal microphytobenthos in sediment
657 depends on the light photoperiod, intensity, and spectrum: evidence for a positive effect
658 of blue wavelengths. *Front Mar Sci* 2020;7:212. 10.3389/fmars.2020.00212
659 20. Cohn S, Manoylov K, Gordon R (eds). Diatom Gliding Motility. John Wiley & Sons, 2021.
660 10.1002/9781119526483
661 21. Morelle J et al. The photoprotective behavior of a motile benthic diatom as elucidated
662 from the interplay between cell motility and physiological responses to a light
663 microgradient using a novel experimental setup. *Microb Ecol* 2024;87:40.
664 10.1007/s00248-024-02354-7
665 22. Poulsen NC et al. Diatom gliding is the result of an actin-myosin motility system. *Cell*
666 *Motil Cytoskeleton* 1999;44:23–33. 10.1002/(SICI)1097-0169(199909)44:1%3C23::AID-
667 CM2%3E3.0.CO;2-D

668 23. Perkins R et al. Vertical cell movement is a primary response of intertidal benthic biofilms
669 to increasing light dose. *Mar Ecol Prog Ser* 2010;416:93–103. 10.3354/meps08787
670 24. Marques Da Silva J, Duarte B, Utkin AB. Travelling expenses: the energy cost of diel
671 vertical migrations of epipelic microphytobenthos. *Front Mar Sci* 2020;7:433.
672 10.3389/fmars.2020.00433
673 25. Suzuki S et al. Rapid transcriptomic and physiological changes in the freshwater pennate
674 diatom *Mayamaea pseudoterrestris* in response to copper exposure. *DNA Res*
675 2022;29:dsac037. 10.1093/dnares/dsac037
676 26. Morelle J et al. Inter-specific variability in photophysiological responses of epipelic
677 diatoms to the actin inhibitor Latrunculin B. *Diatom Res* 2025;40:133–146.
678 10.1080/0269249X.2024.2447333
679 27. Nakov T, Beaulieu JM, Alverson AJ. Accelerated diversification is related to life history
680 and locomotion in a hyperdiverse lineage of microbial eukaryotes (Diatoms,
681 Bacillariophyta). *New Phytol* 2018;219:462–473. 10.1111/nph.15137
682 28. Roy S et al. (eds). Phytoplankton pigments: characterization, chemotaxonomy and
683 applications in oceanography. Cambridge University Press, 2011.
684 10.1017/CBO9780511732263
685 29. Kuczynska P, Jemiola-Rzeminska M, Strzalka K. Photosynthetic pigments in diatoms.
686 *Mar Drugs* 2015;13:5847–5881. 10.3390/md13095847
687 30. Goss R, Jakob T. Regulation and function of xanthophyll cycle-dependent
688 photoprotection in algae. *Photosynth Res* 2010;106:103–122. 10.1007/s11120-010-
689 9536-x
690 31. Latowski D, Kuczyńska P, Strzałka K. Xanthophyll cycle – a mechanism protecting plants
691 against oxidative stress. *Redox Rep* 2011;16:78–90.
692 10.1179/174329211X13020951739938
693 32. Bastos A et al. Light response of karyostrophy in the benthic pennate diatom
694 *Pleurosigma strigosum* (Bacillariophyceae): a complimentary photoprotective process? *J*
695 *Phycol* 2025;61:1140–1152. 10.1111/jpy.70055

696 33. Furukawa T, Watanabe M, Shihira-Ishikawa I. Green- and blue-light-mediated chloroplast
697 migration in the centric diatomPleurosira laevis. *Protoplasma* 1998;203:214–220.
698 10.1007/BF01279479
699 34. Jönsson B, Sundbäck K, Nilsson C. An upright life-form of an epipelic motile diatom: on
700 the behaviour of *Gyrosigma balticum*. *Eur J Phycol* 1994;29:11–15.
701 10.1080/09670269400650421
702 35. Jesus B et al. Microscale imaging sheds light on species-specific strategies for photo-
703 regulation and photo-acclimation of microphytobenthic diatoms. *Environ Microbiol*
704 2023;25:3087–3103. 10.1111/1462-2920.16499
705 36. De Tommasi E et al. Multiple-pathways light modulation in *Pleurosigma strigosum* bi-
706 raphid diatom. *Sci Rep* 2024;14:6476. 10.1038/s41598-024-56206-y
707 37. Nymark M et al. An integrated analysis of molecular acclimation to high light in the
708 marine diatom *Phaeodactylum tricornutum*. *PLoS ONE* 2009;4:e7743.
709 10.1371/journal.pone.0007743
710 38. Lepetit B et al. Evidence for the existence of one antenna-associated, lipid-dissolved and
711 two protein-bound pools of diadinoxanthin cycle pigments in diatoms. *Plant Physiol*
712 2010;154:1905–1920. 10.1104/pp.110.166454
713 39. Valle KC et al. System responses to equal doses of photosynthetically usable radiation of
714 blue, green, and red Light in the marine diatom *Phaeodactylum tricornutum*. *PLoS ONE*
715 2014;9:e114211. 10.1371/journal.pone.0114211
716 40. Walpersdorf E et al. In situ oxygen dynamics and carbon turnover in an intertidal
717 sediment (Skallingen, Denmark). *Mar Ecol Prog Ser* 2017;566:49–65.
718 10.3354/meps12016
719 41. Stoeck T et al. Multiple marker parallel tag environmental DNA sequencing reveals a
720 highly complex eukaryotic community in marine anoxic water. *Mol Ecol* 2010;19:21–31.
721 10.1111/j.1365-294X.2009.04480.x

42. Eilers PHC, Peeters JCH. A model for the relationship between light intensity and the rate of photosynthesis in phytoplankton. *Ecol Modell* 1988;42:199–215. 10.1016/0304-3800(88)90057-9
43. Silsbe GM, Kromkamp JC. Modeling the irradiance dependency of the quantum efficiency of photosynthesis. *Limnol Oceanogr Methods* 2012;10:645–652. 10.4319/lom.2012.10.645
44. Barranguet, Kromkamp J. Estimating primary production rates from photosynthetic electron transport in estuarine microphytobenthos. *Mar Ecol Prog Ser* 2000. doi:10.3354/meps204039
45. Consalvey M et al. PAM fluorescence: a beginners guide for benthic diatoms. *Diatom Res* 2005;20:1–22. 10.1080/0269249X.2005.9705619
46. Christof Klughammer, Ulrich Schreiber. Complementary PS II quantum yields calculated from simple fluorescence parameters measured by PAM fluorometry and the saturation pulse method. *PAM Application Notes* 2008;1:27–35.
47. Brotas V, Plante-Cuny M-R. The use of HPLC pigment analysis to study microphytobenthos communities. *Acta Oecol* 2003;24:S109–S115. 10.1016/S1146-609X(03)00013-4
48. Van Der Loos LM, Nijland R. Biases in bulk: DNA metabarcoding of marine communities and the methodology involved. *Mol Ecol* 2021;30:3270–3288. 10.1111/mec.15592
49. Gaubert-Boussarie J, Prado S, Hubas C. An untargeted metabolomic approach for microphytobenthic biofilms in intertidal mudflats. *Front Mar Sci* 2020;7:250. 10.3389/fmars.2020.00250
50. Underwood GJC, Barnett, M. What determines species composition in microphytobenthic biofilms. *Royal Netherlands Academy of Arts and Sciences* 2006;123–140.
51. Méléder V et al. Spatiotemporal changes in microphytobenthos assemblages in a macrotidal flat (Bourgneuf Bay,France). *J Phycol* 2007;43:1177–1190. 10.1111/j.1529-8817.2007.00423.x

749 52. Farré EM. The brown clock: circadian rhythms in stramenopiles. *Physiol Plant*
750 2020;169:430–441. 10.1111/ppl.13104
751 53. Prins A et al. Effect of light intensity and light quality on diatom behavioral and
752 physiological photoprotection. *Front Mar Sci* 2020;7:203. 10.3389/fmars.2020.00203
753 54. Schneider RJ et al. Species-level variability in extracellular production rates of reactive
754 oxygen species by diatoms. *Front Chem* 2016;4:5. 10.3389/fchem.2016.00005
755 55. Richter PR et al. High light-induced sign change of gravitaxis in the flagellate *euglena*
756 *gracilis* is mediated by reactive oxygen species. *Acta Protozool* 2003;42:197–204.
757 56. Abele-Oeschger D, Tüg H, Röttgers R. Dynamics of UV-driven hydrogen peroxide
758 formation on an intertidal sandflat. *Limnol Oceanogr* 1997;42:1406–1415.
759 10.4319/lo.1997.42.6.1406
760 57. Kottuparambil S et al. UV-B affects photosynthesis, ROS production and motility of the
761 freshwater flagellate, *Euglena agilis* Carter. *Aquat Toxicol* 2012;122–123:206–213.
762 10.1016/j.aquatox.2012.06.002
763 58. Morris JJ, Rose AL, Lu Z. Reactive oxygen species in the world ocean and their impacts
764 on marine ecosystems. *Redox Biol* 2022;52:102285. 10.1016/j.redox.2022.102285
765 59. Mizrachi A et al. Light-dependent single-cell heterogeneity in the chloroplast redox state
766 regulates cell fate in a marine diatom. *eLife* 2019;8:e47732. 10.7554/eLife.47732
767 60. Lavaud J et al. Influence of the diadinoxanthin pool size on photoprotection in the marine
768 planktonic diatom *Phaeodactylum tricornutum*. *Plant Physiol* 2002;129:1398–1406.
769 10.1104/pp.002014
770 61. Waring J et al. Light-induced responses of oxygen photoreduction, reactive oxygen
771 species production and scavenging in two diatom species. *J Phycol* 2010;46:1206–1217.
772 10.1111/j.1529-8817.2010.00919.x
773 62. Rijstenbil JW. UV- and salinity-induced oxidative effects in the marine diatom
774 *Cylindrotheca closterium* during simulated emersion. *Mar Biol* 2005;147:1063–1073.
775 10.1007/s00227-005-0015-4

776 63. Kalaji HM et al. Chlorophyll a fluorescence as a tool to monitor physiological status of
777 plants under abiotic stress conditions. *Acta Physiol Plant* 2016;38:102. 10.1007/s11738-
778 016-2113-y
779 64. Jesus B et al. Effects of vertical migrations by benthic microalgae on fluorescence
780 measurements of photophysiology. *Mar Ecol Prog Ser* 2006;315:55–66.
781 10.3354/meps315055
782 65. Cartaxana P et al. Physiological versus behavioral photoprotection in intertidal epipelic
783 and epipsammic benthic diatom communities. *J Exp Mar Biol Ecol* 2011;405:120–127.
784 10.1016/j.jembe.2011.05.027
785 66. Jesus B et al. Adaptations of microphytobenthos assemblages to sediment type and tidal
786 position. *Cont Shelf Res* 2009;29:1624–1634. 10.1016/j.csr.2009.05.006
787 67. Barnett A et al. Growth form defines physiological photoprotective capacity in intertidal
788 benthic diatoms. *ISME J* 2015;9:32–45. 10.1038/ismej.2014.105
789 68. Cheng K et al. Probing the photochemical formation of hydroxyl radical from dissolved
790 organic matter: insights into the H_2O_2-dependent pathway. *Environ Sci Technol*
791 2025;59:2245–2256. 10.1021/acs.est.4c10348
792 69. Diaz JM, Plummer S. Production of extracellular reactive oxygen species by
793 phytoplankton: past and future directions. *J Plankton Res* 2018;40:655–666.
794 10.1093/plankt/fby039
795 70. Amorim DS et al. Effects of cold plasma on chlorophylls, carotenoids, anthocyanins, and
796 betalains. *Food Res Int* 2023;167:112593. 10.1016/j.foodres.2023.112593
797 71. Ataka R et al. Determination of *N*-centered stereochemistry in N22-methylated
798 chlorophyll-*a* derivatives and their epimer-dependent optical spectra. *Chirality*
799 2024;36:e23681. 10.1002/chir.23681
800 72. Carrara F et al. Bistability in oxidative stress response determines the migration behavior
801 of phytoplankton in turbulence. *Proc Natl Acad Sci USA* 2021;118:e2005944118.
802 10.1073/pnas.2005944118

803 73. De Carpentier F et al. How abiotic stress-induced socialization leads to the formation of
804 massive aggregates in *Chlamydomonas*. *Plant Physiol* 2022;190:1927–1940.
805 10.1093/plphys/kiac321
806 74. Li Z et al. Common environmental stress responses in a model marine diatom. *New*
807 *Phytol* 2023;240:272–284. 10.1111/nph.19147
808 75. Volpert A et al. Diurnal fluctuations in chloroplast GSH redox state regulate susceptibility
809 to oxidative stress and cell fate in a bloom-forming diatom. *J Phycol* 2018;54:329–341.
810 10.1111/jpy.12638
811 76. Pivato M et al. Compartment-specific Ca^{2+} imaging in the green alga *Chlamydomonas*
812 *reinhardtii* reveals high light-induced chloroplast Ca^{2+} signatures. *New Phytol*
813 2023;240:258–271. 10.1111/nph.19142
814 77. Flori S et al. Diatoms exhibit dynamic chloroplast calcium signals in response to high light
815 and oxidative stress. *Plant Physiol* 2025;197:kiae591. 10.1093/plphys/kiae591
816 78. Bienert GP, Chaumont F. Aquaporin-facilitated transmembrane diffusion of hydrogen
817 peroxide. *Biochim Biophys Acta Gen Subj* 2014;1840:1596–1604.
818 10.1016/j.bbagen.2013.09.017
819 79. Pohnert G. Phospholipase A2 Activity Triggers the Wound-Activated Chemical Defense
820 in the Diatom *Thalassiosira rotula*. *Plant Physiol* 2002;129:103–111. 10.1104/pp.010974
821 80. Vardi A et al. A stress surveillance system based on calcium and nitric oxide in marine
822 diatoms. *PLoS Biol* 2006;4:e60. 10.1371/journal.pbio.0040060
823 81. Mukai K et al. Effects of light and hydrogen peroxide on gene expression of newly
824 identified antioxidant enzymes in the harmful algal bloom species *Chattonella marina*.
825 *Eur J Phycol* 2019;54:393–403. 10.1080/09670262.2019.1576062
826 82. Osuna-Cruz CM et al. The *Seminavis robusta* genome provides insights into the
827 evolutionary adaptations of benthic diatoms. *Nat Commun* 2020;11:3320.
828 10.1038/s41467-020-17191-8

83. Russo MT et al. The first genetic engineered system for ovothiol biosynthesis in diatoms reveals a mitochondrial localization for the sulfoxide synthase OvoA. *Open Biol* 2023;13:220309. 10.1098/rsob.220309
84. Bowler C, Fluhr R. The role of calcium and activated oxygens as signals for controlling cross-tolerance. *Trends Plant Sci* 2000;5:241–246. 10.1016/S1360-1385(00)01628-9
85. Morelle J et al. Light induced transthylakoidal proton gradient is a key signal driving the downward migration of motile diatoms in sediments. *Sci Rep* 2025;15:20664. 10.1038/s41598-025-07737-5
86. Pei Z-M et al. Calcium channels activated by hydrogen peroxide mediate abscisic acid signalling in guard cells. *Nature* 2000;406:731–734. 10.1038/35021067
87. Cooksey B, Cooksey KE. Calcium is necessary for motility in the diatom *Amphora coffeaeformis*. *Plant Physiol* 1980;65:129–131. 10.1104/pp.65.1.129
88. McLachlan DH et al. Calcium release from intracellular stores is necessary for the photophobic response in the benthic diatom *Navicula perminuta (Bacillariophyceae)*. *J Phycol* 2012;48:675–681. 10.1111/j.1529-8817.2012.01158.x
89. Helliwell KE et al. Alternative mechanisms for fast Na+/Ca2+ signaling in eukaryotes via a novel class of single-domain voltage-gated channels. *Curr Biol* 2019;29:1503-1511.e6. 10.1016/j.cub.2019.03.041
90. Wu F et al. Hydrogen peroxide sensor HPCA1 is an LRR receptor kinase in *Arabidopsis*. *Nature* 2020;578:577–581. 10.1038/s41586-020-2032-3

SUPPLEMENTARY DATA

Two additional documents: (1) supplementary materials and methods and (2) supplementary data.

FIGURE CAPTIONS

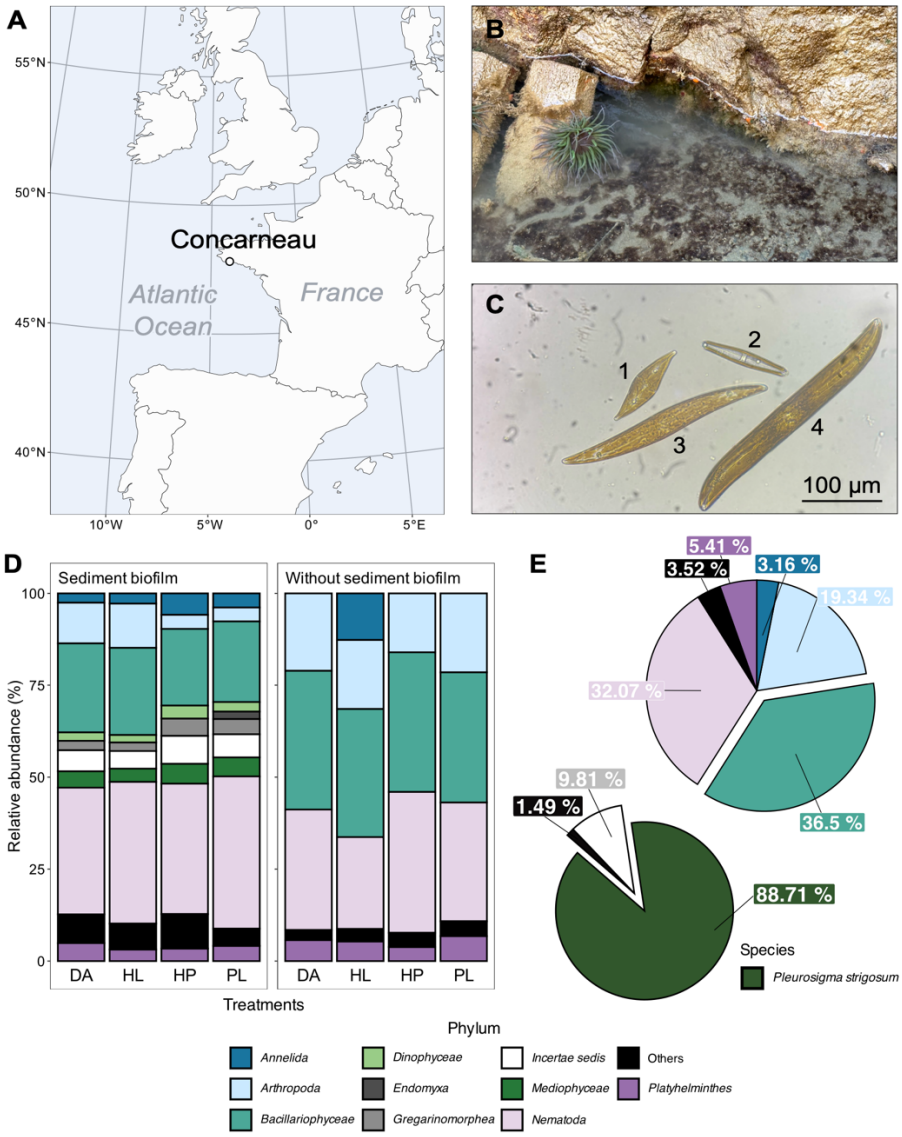

Figure 1. Microphytobenthic community diversity

A. *Geographical location of the studied microphytobenthic biofilm;* ***B.*** *Microphytobenthic biofilm (brown patches) developing on muddy substrata of the breeding pond;* ***C.*** *Light microscopy image of the most commonly observed diatom species in the microphytobenthic community: 1. Pleurosigma* sp.*, 2. Navicula* sp.*, 3. Pleurosigma strigosum, 4. Gyrosigma* sp.*;* ***D.*** *Relative average abundances barplot (%; n = 5 per treatment) of eukaryotic phyla from microphytobenthic samples (some sequences derive from planktonic eDNA, thus contributing to the observed community composition) for Sediment Biofilm (SB) and Without Sediment Biofilm (WSB), under Dark-Adapted control (DA), High Light (HL), Hydrogen Peroxide (HP), and Cold Atmospheric Plasma (PL) treatments;* ***E.*** *Average WSB microphytobenthic community across treatments, highlighting the prevalence of the autotrophic phylum Bacillariophyceae (first pie chart), and the significant contribution of Pleurosigma strigosum within Bacillariophyceae abundances (second pie chart). The "Others" category includes the sum of taxa with <2% abundance.*

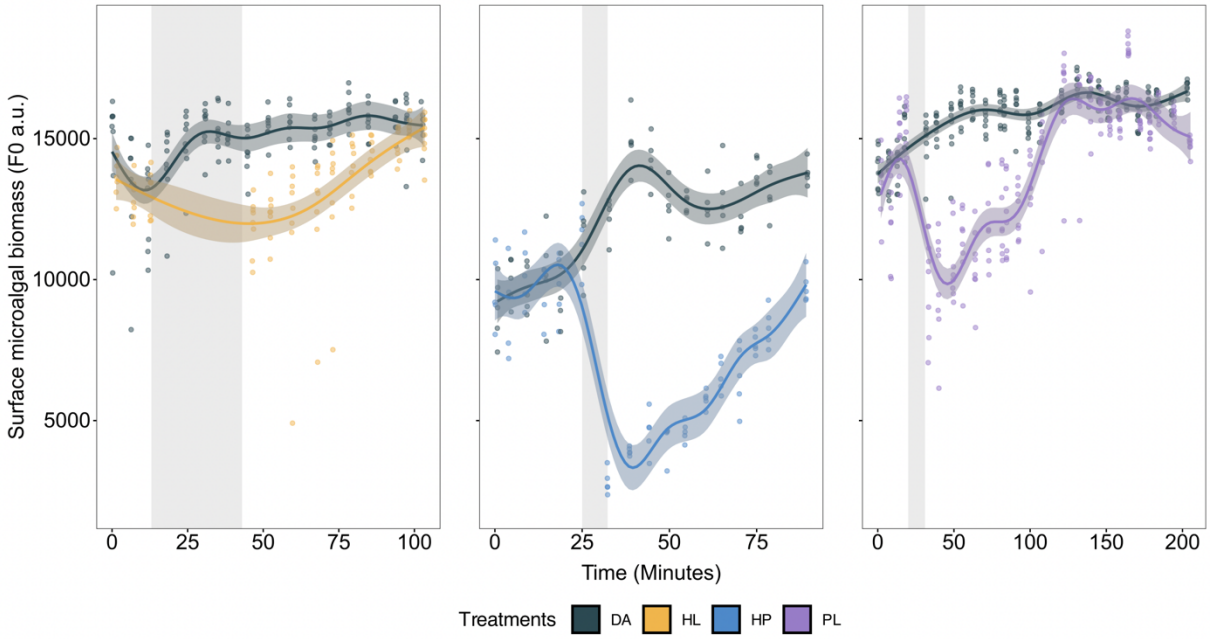

Figure 2. Downward migration of microphytobenthos under the three oxidative stresses

Temporal monitoring of surface microalgal biomass (F_0, arbitrary unit) for the Sediment Biofilm (SB) samples under the three oxidative stresses: High Light (HL; n = 8), Hydrogen Peroxide (HP; n = 5), and Cold Atmospheric Plasma (PL; n = 8), compared to a Dark-Adapted control (DA). Shaded grey areas indicate the stress period. All measurements were taken in the morning, during the upward migration phase of microphytobenthos.

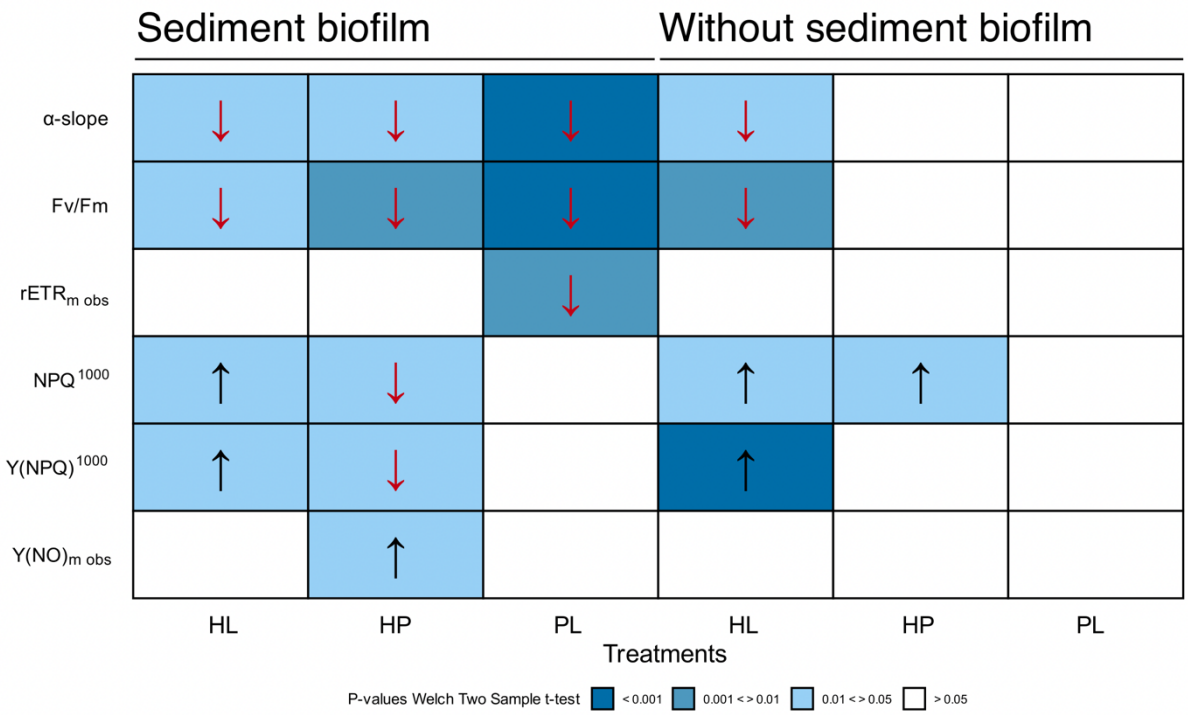

Figure 3. Heatmap of net photophysiological responses under oxidative stresses

Net impact of High Light (HL), Hydrogen Peroxide (HP), and Cold Atmospheric Plasma (PL) treatments on photosynthetic parameters. Welch's two-sample t-test (n = 3) was used to calculate the stress-induced changes $\Delta_{After - Before}$, relative to DA ($\Delta_{After - Before\ DA}$), in order to correct for the natural photophysiological variation observed under the darkness treatment. Arrows indicate the direction of the change induced by each stressor compared to the DA control. α-slope (arbitrary unit). Fv/Fm (unitless) corresponds to the maximum quantum yield of photosystem II photochemistry under dark-adapted state. $rETR_{m\ obs}$ (arbitrary unit) and $Y(NO)_{m\ obs}$ (unitless) refer to the maximum values observed within the measured light curve range (without extrapolation). NPQ^{1000} (unitless) and $Y(NPQ)^{1000}$ (unitless) correspond to the maximum values measured after the final one-minute light curve step at 1000 µmol photons m^{-2} s^{-1} (without extrapolation). All fluorescence measurements were performed on dark-adapted samples for both Sediment Biofilm (SB) and Without Sediment Biofilm (WSB) communities. See supplementary Table 3 and 4 for detailed values.

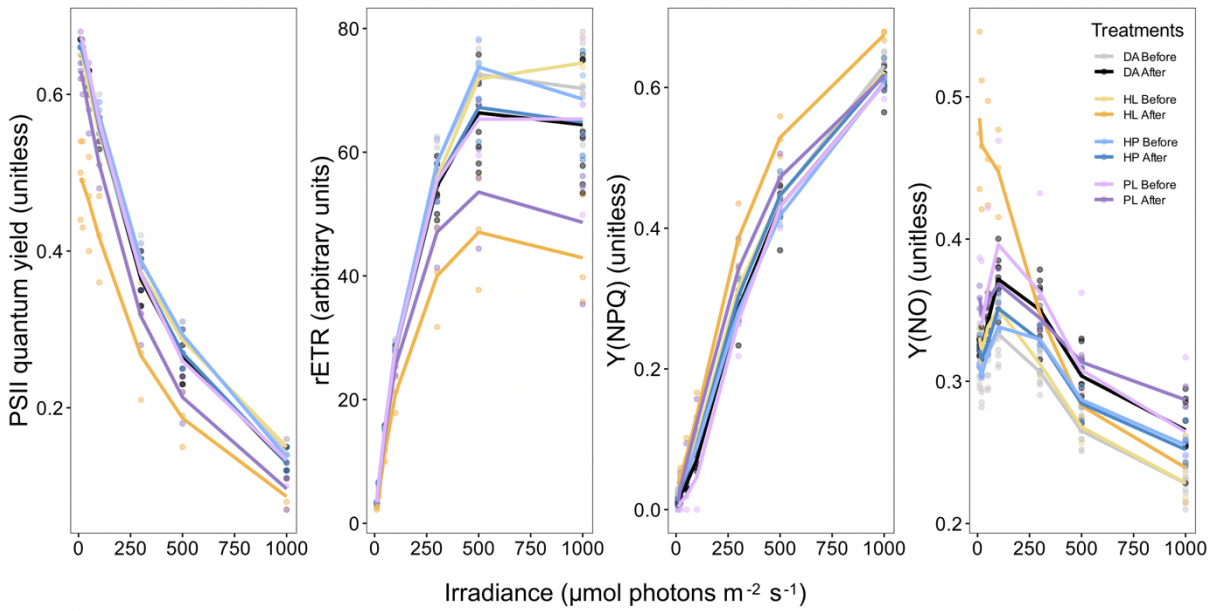

Figure 4. Stress-induced photosynthetic efficiency profiles

Photosystem II (PSII) quantum yield, rETR, Y(NPQ), and Y(NO) response curves of Without Sediment Biofilm (WSB) community, under the three stresses: High Light (HL), Hydrogen Peroxide (HP), and Cold Atmospheric Plasma (PL), compared to the Dark-Adapted control (DA). All photosynthetic parameters measured with n = 3.

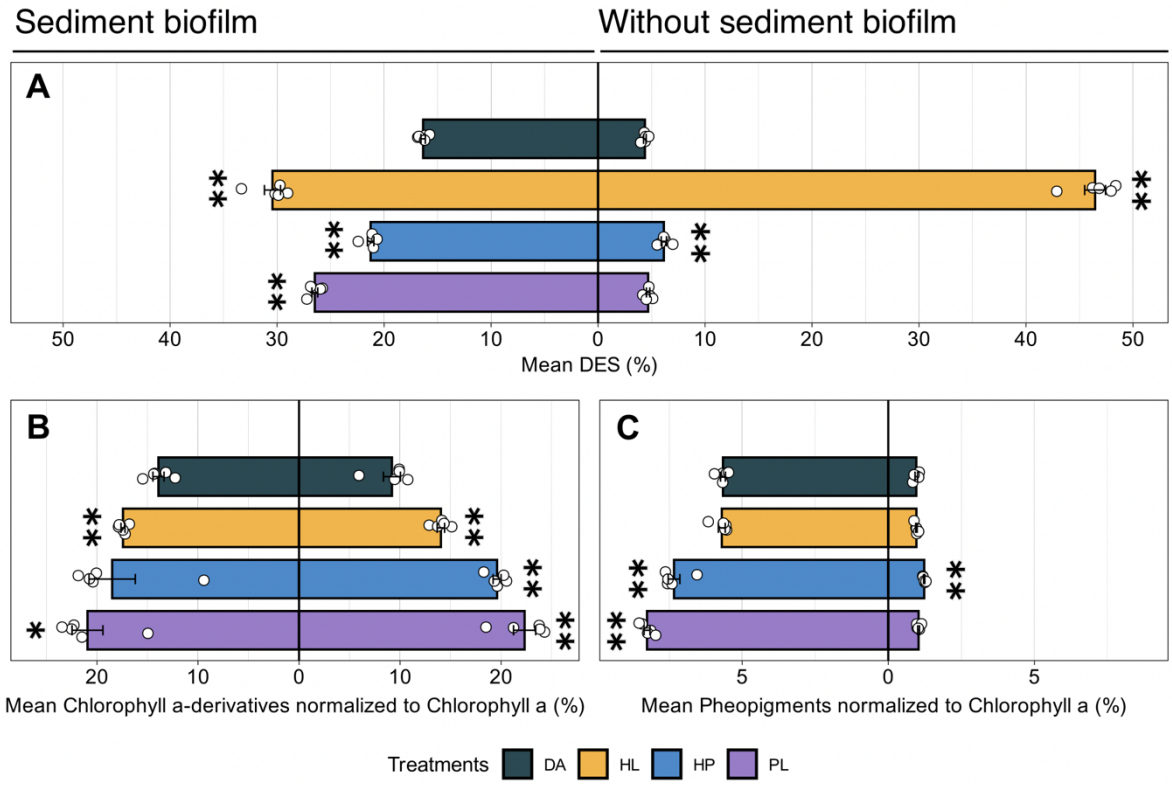

Figure 5. Impact of treatments on pigment content

Barplot showing variations in pigment ratios (%) under the following treatments: Dark-Adapted control (DA), High Light (HL), Hydrogen Peroxide (HP), and Cold Atmospheric Plasma (PL), for both Sediment Biofilm (SB, left panel) and Without Sediment Biofilm (WSB, right panel) communities; ***A.*** *Barplots of the de-epoxidation state DES (%);* ***B.*** *Barplots of Chlorophyll a-derivatives pigment ratios;* ***C.*** *Barplots of Pheopigments pigment ratios. Statistical differences were assessed by the Mann-Whitney U test between DA and each stress (n = 5; P < 0.05 *, < 0.01 **).*

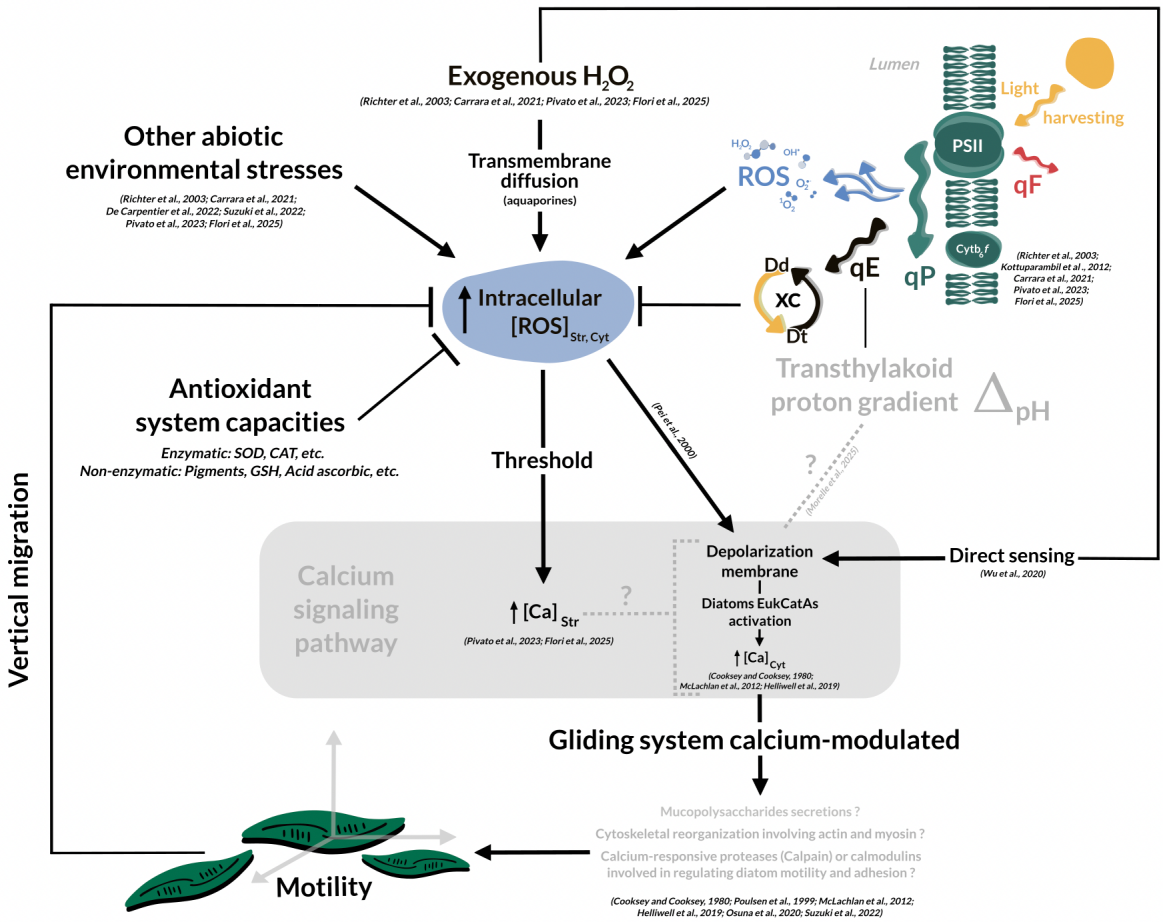

Figure 6. Putative integration of ROS-calcium cellular signaling underlying stress-induced downward vertical migration

Summary of the ROS-Calcium-Motility interplays illustrating a hypothetical signaling model linking the observed motile behavior to the applied stresses. Black arrows and their direction indicate relationships supported by the literature between specific components. Grey dashed lines represent hypothetical interactions. Lines (⊥) indicate processes involved in regulating intracellular ROS concentrations. Abbreviations used in the figure: "qF" fluorescence quenching; "qP" photochemical quenching; "qE" energy-dependent quenching; "str" stromal; "cyt" cytosolic.

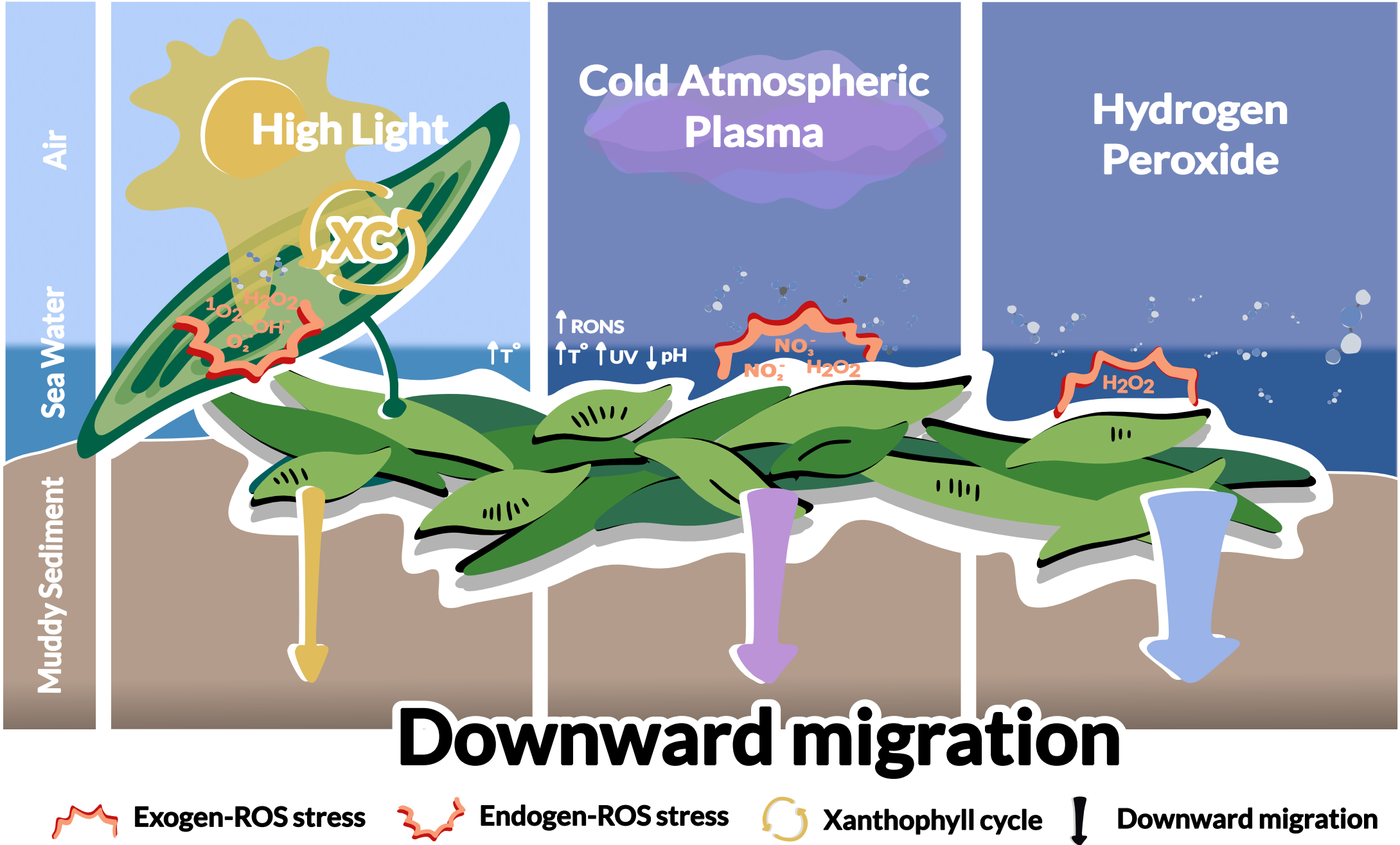
Air
Sea Water
Muddy Sediment
High Light
XC
$^1O_2$
H_2O_2
OH^-
$O_2^{\cdot-}$
↑T°
Cold Atmospheric Plasma
↑RONS
↑T° ↑UV ↓pH
NO_3^-
NO_2^-
H_2O_2
Hydrogen Peroxide
H_2O_2
Downward migration
Exogen-ROS stress
Endogen-ROS stress
Xanthophyll cycle
Downward migration